AIP | Journal of Applied Physics

Temperature and pressure dependent geometry optimization and elastic constant calculations for arbitrary symmetry crystals: Applications to MgSiO3 perovskites

Bin Wen, Tianjiao Shao, Roderick Melnik, Yoshiyuki Kawazoe, and Yongjun Tian

Citation: J. Appl. Phys. **113**, 103501 (2013); doi: 10.1063/1.4794360
View online: http://dx.doi.org/10.1063/1.4794360
View Table of Contents: http://jap.aip.org/resource/1/JAPIAU/v113/i10
Published by the AIP Publishing LLC.

Temperature and pressure dependent geometry optimization and elastic constant calculations for arbitrary symmetry crystals: Applications to $MgSiO_3$ perovskites

Bin Wen,[1,a)] Tianjiao Shao,[2] Roderick Melnik,[3,4] Yoshiyuki Kawazoe,[5] and Yongjun Tian[1]
[1]*State Key Laboratory of Metastable Materials Science and Technology, Yanshan University, Qinhuangdao 066004, China*
[2]*School of Materials Science and Engineering, Dalian University of Technology, Dalian 116023, China*
[3]*M²NeT Lab, Wilfrid Laurier University, Waterloo, 75 University Ave. West, Ontario N2L 3C5, Canada*
[4]*Ikerbasque, Basque Foundation for Science and BCAM, Bilbao 48011, Spain*
[5]*Institute for Materials Research, Tohoku University, 2-1-1 Katahira, Aoba-ku, Sendai 980-8577, Japan*

(Received 5 June 2012; accepted 20 February 2013; published online 8 March 2013)

To optimize lattice parameters for arbitrary symmetry crystals under high temperature and high pressure conditions, a new "geometry optimization method for arbitrary symmetry crystals" has been proposed in this work. By minimizing non-equilibrium Gibbs energy functions for a series of deformed crystal configurations, the components of deformation tensors have been obtained, and allowing the optimized crystal lattice parameters to be determined. Based on our method and Zhao's method, a new method for calculating high temperature and high pressure elastic constants in arbitrary symmetry crystals has been deduced. To verify the effectiveness of the new method, the high temperature and high pressure lattice parameters and elastic constants of orthorhombic symmetry $MgSiO_3$ pv have been studied, and a good agreement between calculated and experimental results has been obtained. © *2013 American Institute of Physics*. [http://dx.doi.org/10.1063/1.4794360]

I. INTRODUCTION

Due to a wide range of industrial applications of high temperature alloys,[1] as well as the important of research on mineral physics of the Earth's interior,[2] high temperature, and high pressure (HTHP) properties of crystals have been a substantial interest for researchers from early 1960s to the present.[3–7] Although many experimental methods have already been developed to study the HTHP properties of crystals,[8–14] it is still difficult and expensive to carry out experimental measurements of HTHP properties of crystals due to complexity of sample preparation and maintaining the sample under high temperature conditions. With the development of computing power, computational methods become an important alternative tool to study the HTHP properties of crystals.[15,16] The geometry optimization of crystals under HTHP conditions is a basis and starting point of the study of HTHP properties of crystals. As a result, this issue has become an important research focus in this field and many geometry optimization methods have been already developed.

To date, density functional theory combined with quasi harmonic approximation (DFT-QHA) method is an effective method for geometry optimization and properties study of crystals under HTHP conditions.[15–31] It has been successfully applied to predict temperature dependent crystal structures and thermal expansion for cubic symmetry crystals.[17–25] Compared with classical molecular dynamics methods which rely on long enough computation times, large enough systems, and accurate potential parameters, the DFT-QHA method, not only accounts for quantum mechanical effects but also accurately and quickly predicts the HTHP crystal structure and some of its properties. In particular, we mention that recently, Wu *et al.* have developed an effective semi-empirical method to compute anharmonic free energy,[26,27] and to extend the DFT-QHA method to accurately predict the HTHP crystals structure and its properties even above its Debye temperature. For example, the computational Clapeyron slope for $\alpha - Mg_2SiO_4$ and $\beta - Mg_2SiO_4$ phases at pressure ranges from 0 to 20 GPa and temperature up to 2500 K can agree well with experimental ones.

Usually, the influence of thermal effects on crystal's lattice parameters is accounted in the DFT-QHA method by minimizing the Gibbs energy as a function of volume at given temperature,[22,23] and this temperature dependent volume are taken as isotropic deformation or the same as the pressure induced crystal cell deformation. For cubic crystals, this hypothesis and treatment are realistic. However, for non-cubic symmetry crystals, the influence of thermal effects on crystal's lattice parameters is not isotropic and also different from the pressure induced deformation mode. Hence, this hypothesis and treatment cannot be applied to non-cubic crystal.[24,25] To overcome this difficulty and to correct errors from isotropic approximations for non-cubic crystals, in 2007, based on the calculation of crystal internal stress and iterative computation, Carrier *et al.*[28,29] relaxed the crystal structure to get zero internal stress and obtained the final optimized HTHP crystal structure. However, since Carrier's method needs internal stress calculation and iterative computation, its computational time increases drastically. To address this problem, a new method has recently been proposed by our group,[32] providing a set of general computational formulas that allow to optimize arbitrary symmetry crystals under HTHP conditions. However, no further details

[a)]Author to whom correspondence should be addressed. Electronic mail: wenbin@ysu.edu.cn. Tel.: 086-335-8568761.

on the application of computational formulas to specific crystals have been given. To fill this gap, a set of computational formulas specific to crystal geometry optimization has been derived in this work, and a new "geometry optimization method for arbitrary symmetry crystals" has been proposed to perform lattice parameters optimization for arbitrary symmetry crystals under HTHP conditions. More specifically, based on the geometry optimization, a computational method for determining HTHP elastic constants for arbitrary symmetry crystals has been developed. To illustrate its general applicability, the crystal parameters and elastic constants for orthorhombic $MgSiO_3$ perovskite ($MgSiO_3$ pv) have been calculated by using this newly developed methodology.

$MgSiO_3$ is one of the most important mineral composing Earth's structure, its phase diagram and thermodynamic properties have been extensively studied previously.[33–68] $MgSiO_3$ has three well known modifications: $MgSiO_3$ ilmenite with $R\bar{3}c$ symmetry, $MgSiO_3$ perovskite with Pbnm symmetry, and $MgSiO_3$ post-perovskite with Cmcm symmetry. $MgSiO_3$ ilmenite is thermodynamically stable phase of $MgSiO_3$ at atmospheric pressure. When the pressure is above ~30 GPa, a high pressure phase of $MgSiO_3$: $MgSiO_3$ pv, becomes thermodynamically stable phase.[41,45,46] When the pressure is above ~83.7 GPa,[47] $MgSiO_3$ post-perovskite becomes thermodynamically more stable than $MgSiO_3$ pv.[47,48]

Besides of experimental studies for $MgSiO_3$ pv's property,[51–56] a number of theoretical work have been also performed.[25,28–30,59–68] For example, in 2000, Phonon dispersions of $MgSiO_3$ pv has been calculated by Karki *et al.* by using DFT-QHA, and the equation of state, heat capacity, and entropy of $MgSiO_3$ pv have been derived.[25] In 2001, the equation of state, thermal expansion coefficients (TEC), Gruneisen parameter, and elastic constants of $MgSiO_3$-pv have been studied by using *ab initio* molecular dynamic simulation by Oganov *et al.*[59,60] In 2004, isentropic elastic constants of $MgSiO_3$ pv at pertinent pressures and temperatures have been predicted by using DFT-QHA by Wentzcovitch *et al.*[30] At the same year, Qin has predicted the structure distortion of $MgSiO_3$ pv at high pressure.[63] In 2012, Metsue and Tsuchiya investigated the thermodynamic properties of (Mg, Fe)SiO_3 perovskite at the lower mantle pressures and temperatures, iron is incorporated in the high and low spin states for the first time in the calculation.[68]

Although the previous experimental and theoretical work contributes a sound and steady progress, to the best of our knowledge, the anisotropic temperature dependent linear TEC of $MgSiO_3$ has never been reported. Here, we would like to report a systematically investigation on temperature and pressure dependent lattice parameters, phonon dispersion curves, linear and volume TEC, isothermal, and isentropic elastic constants of $MgSiO_3$ pv.

The paper is organized as follows. Section II introduces our crystal geometry optimization and elastic constant computation for arbitrary symmetry crystals under HTHP conditions. Section III discusses the results obtained by this method for temperature and pressure dependent geometry optimization and elastic constants for orthorhombic $MgSiO_3$ pv. It also provides details of comparisons with experimental results. Conclusions are given in Sec. IV.

II. THEORETICAL METHODOLOGY

A. Temperature and pressure dependent geometry optimization method

In the following, we demonstrate our methodology called the "geometry optimization method for arbitrary symmetry crystals" (the GOMASC method) to perform temperature and pressure dependent geometry optimization for arbitrary symmetry crystals. Based on the linear algebra and tensor analysis ideas and crystallographic theory,[69,70] a deformed crystal configuration tensor can be expressed as a function of an initial crystal configuration tensor and a second order strain tensor ε. Therefore, the deformed crystal configuration tensor X can be expressed as

$$X = \begin{pmatrix} a_1' \\ a_2' \\ a_3' \end{pmatrix} = \begin{pmatrix} a_1 \\ a_2 \\ a_3 \end{pmatrix} \cdot (1+\varepsilon), \tag{1}$$

where a_i are the primitive vectors and

$$\varepsilon = \begin{pmatrix} e_{xx} & \frac{e_{xy}}{2} & \frac{e_{zx}}{2} \\ \frac{e_{xy}}{2} & e_{yy} & \frac{e_{yz}}{2} \\ \frac{e_{zx}}{2} & \frac{e_{yz}}{2} & e_{zz} \end{pmatrix}, \tag{2}$$

where the strain components, e_{ij}, are defined in Cartesian coordinates.

Further, the deformed configuration tensor induced by temperature and pressure can be expressed as a function of the initial crystal configuration tensor and a strain tensor $\varepsilon(P,T)$ at pressure P and temperature T conditions.

$$X(P,T) = \begin{pmatrix} a_1(P,T) \\ a_2(P,T) \\ a_3(P,T) \end{pmatrix} = \begin{pmatrix} a_1 \\ a_2 \\ a_3 \end{pmatrix} \cdot [1+\varepsilon(P,T)], \tag{3}$$

$$\text{where } \varepsilon(P,T) = \begin{pmatrix} e_{xx}(P,T) & \frac{e_{xy}(P,T)}{2} & \frac{e_{zx}(P,T)}{2} \\ \frac{e_{xy}(P,T)}{2} & e_{yy}(P,T) & \frac{e_{yz}(P,T)}{2} \\ \frac{e_{zx}(P,T)}{2} & \frac{e_{yz}(P,T)}{2} & e_{zz}(P,T) \end{pmatrix}, \tag{4}$$

where the strain component, $e_{ij}(P,T)$, is a function of both temperature and pressure.

If the deformation is performed under isobaric conditions, the Eq. (3) can be rewritten as

$$X^P(T) = \begin{pmatrix} a_1^P(T) \\ a_2^P(T) \\ a_3^P(T) \end{pmatrix} = \begin{pmatrix} a_1 \\ a_2 \\ a_3 \end{pmatrix} \cdot [1+\varepsilon^P(T)], \tag{5}$$

$$\text{where } \varepsilon^P(T) = \begin{pmatrix} {e_{xx}}^P(T) & \frac{{e_{xy}}^P(T)}{2} & \frac{{e_{zx}}^P(T)}{2} \\ \frac{{e_{xy}}^P(T)}{2} & {e_{yy}}^P(T) & \frac{{e_{yz}}^P(T)}{2} \\ \frac{{e_{zx}}^P(T)}{2} & \frac{{e_{yz}}^P(T)}{2} & {e_{zz}}^P(T) \end{pmatrix}, \tag{6}$$

where the strain component, $e_{ij}{}^{P}(T)$, is a function of only temperature.

Because many crystals usually have thermal expansion coefficients that do not vary significantly over the range of temperatures,[71] to simplify calculation process, in this work, we assume that ratios $e^{P}_{xy}(T)$, $e^{P}_{zx}(T)$, $\alpha^{P}_{yy}(T)$, $\alpha^{P}_{yz}(T)$, $\alpha^{P}_{zz}(T)$, to $\alpha^{P}_{xx}(T)$ are constants. Therefore, the Eq. (5) can be approximated by

$$X^{P}(T) = \begin{pmatrix} a_1 \\ a_2 \\ a_3 \end{pmatrix} \left(1 + e^{P}_{xx}(T) \begin{bmatrix} 1 & f & e \\ f & b & d \\ e & d & c \end{bmatrix} \right), \quad (7)$$

where b, c, d, e, and f are constants, independent of temperature.

Therefore, on the basis of standard thermodynamics arguments,[72,73] for the deformed crystal configuration tensor $X^{P}(T)$ in Eq. (7), its non-equilibrium Gibbs energy $G[X^{P}(T);T]$ is given by

$$G[X^{P}(T);T] = E\{X^{P}[e^{P}_{xx}(T)]\} + PV\{X^{P}[e^{P}_{xx}(T)\} - TS, \quad (8)$$

where $X^{P}(T)$ represents the deformed crystal configuration tensor induced by pressure P and temperature T conditions. $E\{X^{P}[e^{p}_{xx}(T)]\}$ and $V\{X^{P}[\alpha^{p}_{xx}(T)]\}$ are the total energy and volume of the unit cell for the deformed crystal configuration tensor $X^{P}(T)$, respectively. S is the total entropy.

If only vibrational entropy be considered here, the Eq. (8) can be rewritten as

$$G[X^{P}(T);T] = E\{X^{P}[e^{P}_{xx}(T)]\} + PV\{X^{P}[e^{P}_{xx}(T)\} + A_{vib}\{X^{P}[e^{P}_{xx}(T)];T\}, \quad (9)$$

where $A_{vib}\{X^{P}[e^{P}_{xx}(T)];T\}$ stands for vibrational Helmholtz free energy, which can be calculated from the QHA method as the following formula:[74,75]

$$A_{vib} = \frac{1}{2}\sum_{q,v} \hbar w_{q,v} - k_B T \sum_{q,v} \ln[1 - \exp(-\hbar w_{q,v}/k_B T)], \quad (10)$$

where ω is the phonon frequency, T is the temperature, k and $\hbar$ are the Boltzmann constant and the reduced Planck constant, respectively.

On the basis of Wang's theory,[76] if the deformation tensor is symmetric, the equilibrium Gibbs energy can be obtained by minimizing formula (9) with respect to variable e^{P}_{xx}

$$G*[e^{p,T}_{xx};T) = \min_{e^{p}_{xx}}\{E[X(e^{P}_{xx})] + PV[X(e^{P}_{xx})] + A_{vib}[X(e^{P}_{xx});T]\}, \quad (11)$$

and the corresponding equilibrium strain component $e^{P,T}_{xx}$ at the given pressure P and temperature T can be obtained. Then, if we want to obtain an equilibrium crystal configuration at pressure P and temperature T conditions, we need to obtain every component in the Eq. (7). It is well known that the crystal configuration tensor at pressure P and temperature $T = 0\,\mathrm{K}$ can be obtained by using a general first principle calculation. Recall that there are six unknown components in Eq. (7), which are $e^{P}_{xx}(T)$, b, c, d, e, and f. Because b, c, d, e, and f are not dependent on temperature, if they are determined in advance, $e^{P}_{xx}(T)$ can then be easily obtained by minimizing Eq. (9). Therefore, the focus of the problem is to get reasonable values of b, c, d, e, and f.

In this work, we build a series of strain tensors to determine values of b, c, d, e, and f. For instance, taking strain tensor $\begin{bmatrix} e^{p}_{xx}(T) & 0 & 0 \\ 0 & 0 & 0 \\ 0 & 0 & 0 \end{bmatrix}$ and by minimizing non-equilibrium Gibbs energy of the corresponding deformed configuration tensor, the value of $e^{P,T}_{xx}$ at equilibrium state can be obtained, according to Eq. (11). The value of $e^{P,T}_{yy}$ at equilibrium state can also be obtained by minimizing non-equilibrium Gibbs energy of the deformed configuration on deformation tensor $\begin{bmatrix} 0 & 0 & 0 \\ 0 & e^{p}_{yy}(T) & 0 \\ 0 & 0 & 0 \end{bmatrix}$, and further the ratio of $e^{P}_{yy}(T)$ to $e^{P}_{xx}(T)$, that gives us constant b, can be obtained. By using the same method, the others constants c, d, e, and f can also be obtained.

After constants b, c, d, e, and f are determined, we reuse the Eq. (11) to obtain a more accurate value of $e^{P}_{xx}(T)$ at equilibrium state. At this step, a preliminary equilibrium HTHP crystal structure is obtained. If we want to obtain even more accurate results, we can recalculate the values of b, c, d, e, and f by using the values of b, c, d, e, and f obtained at the previous step. For example, $e^{P}_{xx}(T)$ and $e^{P}_{yy}(T)$ at equilibrium state can be obtained by minimizing non-equilibrium Gibbs energy of deformed configuration tensors $\begin{bmatrix} e^{p}_{xx}(T) & f_1 & e_1 \\ f_1 & b_1 & d_1 \\ e_1 & d_1 & c_1 \end{bmatrix}$ and $\begin{bmatrix} a_1/b_1 & f_1/b_1 & e_1/b_1 \\ f_1/b_1 & e^{p}_{xx}(T) & d_1/b_1 \\ e_1/b_1 & d_1/b_1 & c_1/b_1 \end{bmatrix}$, where b_1, c_1, d_1, e_1, and f_1 are the values of b, c, d, e, and f, obtained at the previous step. Further the ratio of $e^{P}_{yy}(T)$ to $e^{P}_{xx}(T)$ can be obtained, that is a more accurate value of b. By the same way, the more accurate values for the other constants c, d, e, and f can also be obtained. By repeating iterative calculations, we can reach any prescribed accuracy for predicting HTHP crystal structures.

It is worthy mentioning that for crystals with different symmetry, the number of independent lattice parameters is reduced. Therefore, the strain tensor can be simplified. The details of strain tensors for crystals with different symmetries have been listed in Table I.

B. Temperature and pressure dependent elastic constants calculation

On the basis of the optimized HTHP crystal structure by applying our GOMASC method, the HTHP elastic constants can be calculated with help of Zhao's method. In 2007, Zhao *et al.* proposed a general methodology for calculating a complete set of second order isothermal elastic constants for arbitrary symmetry crystals[77] by combing first-principles calculations and continuum elasticity theory.[78,79] The details of calculation processing can be described as follows.

TABLE I. Strain tensors used to perform geometry optimization for seven kinds of crystal symmetry.

Crystal system	Crystal lattice	Strain tensor	Number of deformation tensor used
Triclinic	$a \neq b \neq c$ $\alpha \neq \beta \neq \gamma$	$\begin{bmatrix} \alpha_1 & \alpha_6 & \alpha_5 \\ \alpha_6 & \alpha_2 & \alpha_4 \\ \alpha_5 & \alpha_4 & \alpha_3 \end{bmatrix}$	6
Monoclinic	$a \neq b \neq c$ $\alpha = \beta = 90^\circ \neq \gamma$	$\begin{bmatrix} \alpha_1 & 0 & 0 \\ 0 & \alpha_2 & \alpha_4 \\ 0 & \alpha_4 & \alpha_3 \end{bmatrix}$	4
Orthorhombic	$a \neq b \neq c$ $\alpha = \beta = \gamma = 90^\circ$	$\begin{bmatrix} \alpha_1 & 0 & 0 \\ 0 & \alpha_2 & 0 \\ 0 & 0 & \alpha_3 \end{bmatrix}$	3
Trigonal	$a = b = c$ $\alpha = \beta = \gamma \neq 90^\circ$	$\begin{bmatrix} \alpha_1 & \alpha_4 & \alpha_4 \\ \alpha_4 & \alpha_1 & \alpha_4 \\ \alpha_4 & \alpha_4 & \alpha_1 \end{bmatrix}$	2
Tetragonal	$a = b \neq c$ $\alpha = \beta = \gamma = 90^\circ$	$\begin{bmatrix} \alpha_1 & 0 & 0 \\ 0 & \alpha_1 & 0 \\ 0 & 0 & \alpha_3 \end{bmatrix}$	2
Hexagonal	$a = b \neq c$ $\alpha = \beta = 90^\circ\ \gamma = 120^\circ$	$\begin{bmatrix} \frac{\sqrt{3}}{2}\alpha_1 & -\frac{1}{2}\alpha_1 & 0 \\ 0 & \alpha_1 & 0 \\ 0 & 0 & \alpha_3 \end{bmatrix}$	2
Cubic	$a = b = c$ $\alpha = \beta = \gamma = 90^\circ$	$\begin{bmatrix} \alpha_1 & 0 & 0 \\ 0 & \alpha_1 & 0 \\ 0 & 0 & \alpha_1 \end{bmatrix}$	1

For a deformed HTHP crystal configuration $X^{P,T}(\xi)$ obtained by a special strain tensor with strain ξ, its Helmholtz free energy is

$$F[X^{P,T}(\xi);T] = E[X^{P,T}(\xi)] + A_{vib}[X^{P,T}(\xi);T], \tag{12}$$

where $E[X^{P,T}(\xi)]$ is the total energy and $A_{vib}[X^{P,T}(\xi);T]$ is the vibrational Helmholtz free energy, which can also be calculated from phonon density of states by using the QHA method or a first principles molecular dynamics method.[74,75]

Therefore, under pressure P and temperature T conditions, the Helmholtz free energy for a deformed HTHP crystal configuration is a function of one variable ξ. Hence, Eq. (12) can be expanded as a Taylor series in variable ξ at a constant temperature

$$\begin{aligned} F[X^{P,T}(\xi);T] = {} & F[X^{P,T}(0);T] + \left.\frac{dF[X^{P,T}(\xi);T]}{d\xi}\right|_{\xi=0} \xi \\ & + \left.\frac{d^2F[X^{P,T}(\xi);T]}{2!d\xi^2}\right|_{\xi=0} \xi^2 \\ & + \cdots + \left.\frac{d^nF[X^{P,T}(\xi);T]}{n!d\xi^2}\right|_{\xi=0} \xi^n + R_n(\xi), \end{aligned} \tag{13}$$

and the second order strain derivatives of the Helmholtz free energy $\frac{d^2F[X^{P,T}(\xi);T]}{d\xi^2}$ equals to a linear combination of isothermal elastic constants (LCIEC). These relationships between second order strain derivatives of the Helmholtz free energy and LCIEC for different symmetries at different deformation mode have been listed in Table II.[80,81]

Thus, in order to determine the elastic constants for a crystal under HTHP conditions, a series of deformed crystals need to be built and the corresponding second order strain derivatives of the Helmholtz free energy need to be derived by, e.g., the polynomial fitting technique. Further, the isothermal elastic constants can be obtained by solving a system of linear equations giving the relationship between these second order strain derivatives of the Helmholtz free energy and LCIEC. It is worth mentioning that, to calculate the shear elastic constants like c_{44}, c_{55}, and c_{66}, volume conserving deformations are applied. Since energy is a function of both deformation strain and volume. Therefore, volume-conserving deformation modes enable us to obtain elastic constants with high accuracy since the energy of deformed unit cell depends only on distortion.[82,83]

On the basis of isothermal elastic constants, isentropic elastic constants can be calculated through the thermodynamic relations proposed by Davies[84]

$$c_{ij}^S = c_{ij}^T + \frac{TV\lambda_i\lambda_j}{C_V}, \tag{14}$$

TABLE II. Strain tensors used to calculate the complete set of independent second order elastic constants for all seven kinds of lattice symmetry. LCIEC equal to second order strain derivatives of the Helmholtz free energy under the corresponding deformation modes (or strain tensors).[80,81]

Crystal symmetry	Strain tensor	LCEC
Cubic symmetry	$[\delta,-\delta,\delta^2/(1-\delta^2),0,0,0]$	$2c_{11}-2c_{12}$
	$[\delta^2/(1-\delta^2),0,0,2\delta,0,0]$	$4c_{44}$
	$[\delta,\delta,\delta,0,0,0]$	$3c_{11}+6c_{12}$
Hexagonal symmetry	$[\delta,\delta,\delta,0,0,0]$	$2c_{11}+c_{33}+2c_{12}+4c_{13}$
	$[\delta,-\delta,\delta^2/(1-\delta^2),0,0,0]$	$2c_{11}-2c_{12}$
	$[\delta,\delta,0,0,0,0]$	$2c_{11}+2c_{12}$
	$[\delta,\delta^2/(1-\delta^2),-\delta,0,0,0]$	$c_{11}+c_{33}-2c_{13}$
	$[\delta^2/(1-\delta^2),0,0,2\delta,0,0]$	$4c_{44}$
Trigonal Symmetry	$[\delta,-\delta,\delta^2/(1-\delta^2),0,0,0]$	$2c_{11}-2c_{12}$
	$[\delta,\delta^2/(1-\delta^2),-\delta,0,0,0]$	$c_{11}+c_{33}-2c_{13}$
	$[\delta,\delta,0,0,0,0]$	$2c_{11}+2c_{12}$
	$[\delta,0,\delta,0,0,0]$	$c_{11}+c_{33}+2c_{13}$
	$[\delta,0,0,2\delta,0,0]$	$c_{11}+4c_{44}+4c_{14}$
	$[\delta,0,0,-2\delta,0,0]$	$c_{11}+4c_{44}-4c_{14}$
Tetragonal Symmetry	$[\delta,-\delta,\delta^2/(1-\delta^2),0,0,0]$	$c_{11}+c_{22}-2c_{12}$
	$[\delta,\delta^2/(1-\delta^2),-\delta,0,0,0]$	$c_{11}+c_{33}-2c_{13}$
	$[\delta,\delta,0,0,0,0]$	$c_{11}+c_{22}+2c_{12}$
	$[\delta,0,\delta,0,0,0]$	$c_{11}+c_{33}+2c_{33}$
	$[\delta^2/(1-\delta^2),0,0,2\delta,0,0]$	$4c_{44}$
	$[0,0,\delta^2/(1-\delta^2),0,0,2\delta]$	$4c_{66}$
Orthorhombic Symmetry	$[\delta,\delta,0,0,0,0]$	$c_{11}+c_{22}+2c_{12}$
	$[\delta,0,\delta,0,0,0]$	$c_{11}+c_{33}+2c_{13}$
	$[0,\delta,\delta,0,0,0]$	$c_{22}+c_{33}+2c_{23}$
	$[\delta,-\delta,\delta^2/(1-\delta^2),0,0,0]$	$c_{11}+c_{22}-2c_{12}$
	$[\delta,\delta^2/(1-\delta^2),-\delta,0,0,0]$	$c_{11}+c_{33}-2c_{13}$
	$[\delta^2/(1-\delta^2),\delta,-\delta,0,0,0]$	$c_{22}+c_{33}-2c_{23}$
	$[\delta^2/(1-\delta^2),0,0,2\delta,0,0]$	$4c_{44}$
	$[0,\delta^2/(1-\delta^2),0,0,2\delta,0]$	$4c_{55}$
	$[0,0,\delta^2/(1-\delta^2),0,0,2\delta]$	$4c_{66}$
Monoclinic Symmetry	$[\delta,\delta,\delta,0,0,0]$	$c_{11}+c_{22}+c_{33}+2c_{12}+2c_{13}+2c_{23}$
	$[\delta,-\delta,\delta^2/(1-\delta^2),0,0,0]$	$c_{11}+c_{22}-2c_{12}$
	$[\delta,\delta^2/(1-\delta^2),-\delta,0,0,0]$	$c_{11}+c_{33}-2c_{13}$
	$[\delta,\delta,0,0,0,0]$	$c_{11}+c_{22}+2c_{12}$
	$[\delta,0,\delta,0,0,0]$	$c_{11}+c_{33}+2c_{13}$
	$[0,\delta,\delta,0,0,0]$	$c_{22}+c_{33}+2c_{23}$
	$[\delta^2/(1-\delta^2),\delta,-\delta,0,0,0]$	$c_{22}+c_{33}-2c_{23}$
	$[\delta^2/(1-\delta^2),0,0,2\delta,0,0]$	$4c_{44}$
	$[\delta,0,0,0,2\delta,0]$	$c_{11}+4c_{55}+4c_{15}$
	$[\delta,0,0,0,-2\delta,0]$	$c_{11}+4c_{55}-4c_{15}$
	$[0,\delta,0,0,2\delta,0]$	$c_{22}+4c_{55}+4c_{25}$
	$[0,0,\delta,0,2\delta,0]$	$c_{33}+4c_{55}+4c_{35}$
	$[0,0,0,\delta,0,\delta]$	$c_{44}+c_{66}+2c_{46}$
	$[0,0,0,\delta,0,-\delta]$	$c_{44}+c_{66}-2c_{46}$
Trinclinic symmetry	$[\delta,\delta,\delta,0,0,0]$	$c_{11}+c_{22}+c_{33}+2c_{12}+2c_{13}+2c_{23}$
	$[\delta,-\delta,\delta^2/(1-\delta^2),0,0,0]$	$c_{11}+c_{22}-2c_{12}$
	$[\delta,\delta^2/(1-\delta^2),-\delta,0,0,0]$	$c_{11}+c_{33}-2c_{13}$
	$[\delta,\delta,0,0,0,0]$	$c_{11}+c_{22}+2c_{12}$
	$[\delta,0,\delta,0,0,0]$	$c_{11}+c_{33}+2c_{13}$
	$[\delta,0,\delta,0,0,0]$	$c_{22}+c_{33}+2c_{23}$
	$[\delta^2/(1-\delta^2),\delta,-\delta,0,0,0]$	$c_{22}+c_{33}-2c_{23}$
	$[\delta,0,0,-2\delta,0,0]$	$c_{11}+4c_{44}-4c_{14}$
	$[\delta,0,0,2\delta,0,0]$	$c_{11}+4c_{44}+4c_{14}$
	$[0,\delta,0,2\delta,0,0]$	$c_{22}+4c_{44}+4c_{24}$
	$[0,0,\delta,2\delta,0,0]$	$c_{33}+4c_{44}+4c_{34}$
	$[\delta,0,0,0,-2\delta,0]$	$c_{11}+4c_{55}-4c_{15}$
	$[\delta,0,0,0,2\delta,0]$	$c_{11}+4c_{55}+4c_{15}$
	$[0,\delta,0,0,2\delta,0]$	$c_{22}+4c_{55}+4c_{25}$
	$[0,0,\delta,0,2\delta,0]$	$c_{33}+4c_{55}+4c_{35}$
	$[0,0,0,\delta,\delta,0]$	$c_{44}+c_{55}+2c_{45}$
	$[\delta,0,0,0,0,-2\delta]$	$c_{11}+4c_{66}-4c_{16}$
	$[\delta,0,0,0,0,2\delta]$	$c_{11}+4c_{66}+4c_{16}$
	$[0,\delta,0,0,0,2\delta]$	$c_{22}+4c_{66}+4c_{26}$
	$[0,0,\delta,0,0,2\delta]$	$c_{33}+4c_{66}+4c_{36}$
	$[0,0,0,\delta,0,\delta]$	$c_{44}+c_{66}+2c_{46}$
	$[0,0,0,0,\delta,\delta]$	$c_{55}+c_{66}+2c_{56}$

$$\lambda_i = -\sum_{j=1}^{6} \alpha_j c_{ij}^T, \tag{15}$$

where T, V, and C_V are temperature, volume, and heat capacity for the unit cell at the given temperature T and pressure p. α_j is the linear thermal expansion coefficient along the direction of deformation strain.

Since the heat capacity can be calculated by integrating density of phonon, and the linear thermal expansion coefficients along different directions can be obtained by our GOMASC method, the isentropic elastic constants can be obtained.

III. APPLICATION

A. Temperature and pressure dependent geometry optimization of orthorhombic $MgSiO_3$ pv

To verify the effectiveness of the GOMASC method, HTHP orthorhombic $MgSiO_3$ pv crystal lattice parameters have been calculated by using this method. Because $MgSiO_3$ pv is orthorhombic, $\begin{bmatrix} e_{xx} & 0 & 0 \\ 0 & e_{yy} & 0 \\ 0 & 0 & e_{zz} \end{bmatrix}$ was chosen as the strain tensor. Therefore, the Eq. (7) can be simplified as follow

$$X^P(T) = \begin{pmatrix} a_1 \\ a_2 \\ a_3 \end{pmatrix} \left(1 + e_{xx}^P(T) \begin{bmatrix} 1 & 0 & 0 \\ 0 & b & 0 \\ 0 & 0 & c \end{bmatrix} \right). \tag{16}$$

There are three independent variables to be determined. Hence, in this work, three strain tensors $\begin{bmatrix} e_{xx}^P(T) & 0 & 0 \\ 0 & 0 & 0 \\ 0 & 0 & 0 \end{bmatrix}$, $\begin{bmatrix} 0 & 0 & 0 \\ 0 & e_{yy}^P(T) & 0 \\ 0 & 0 & 0 \end{bmatrix}$, and $\begin{bmatrix} 0 & 0 & 0 \\ 0 & 0 & 0 \\ 0 & 0 & e_{zz}^P(T) \end{bmatrix}$ were built to determine values of $e_{xx}^p(T)$, b, c. By minimizing non-equilibrium Gibbs energy of the corresponding three deformed configuration tensors, three equilibrium values for variables $e_{xx}^p(T)$, $e_{yy}^p(T)$, and $e_{zz}^p(T)$, namely $e_{xx}^{P,T}$, $e_{yy}^{P,T}$, and $e_{zz}^{P,T}$, can be obtained, according to Eq. (11). Further, the constant b and c can be calculated by calculating the ratio of $e_{yy}^{P,T}/e_{xx}^{P,T}$ and

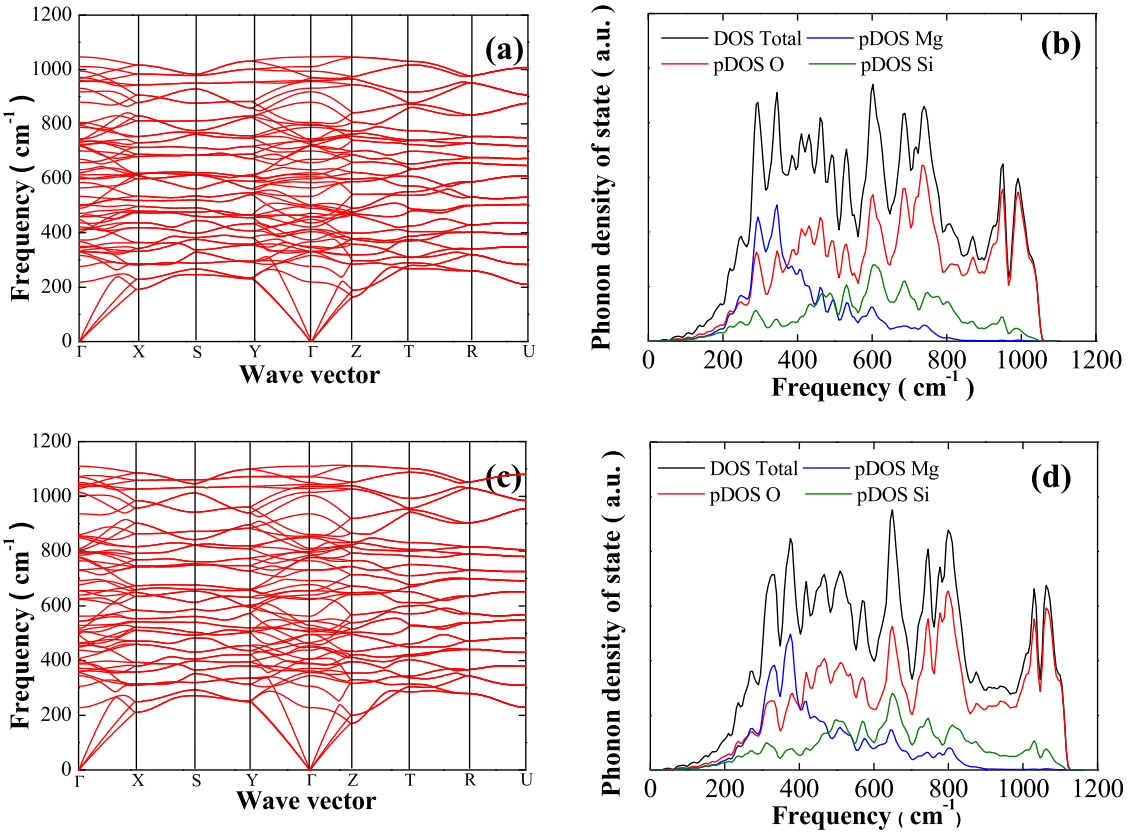

FIG. 1. Phonon dispersion curves and density of states for $MgSiO_3$. (a) Phonon dispersion curves at 0 GPa, (b) phonon density of states at 0 GPa, (c) phonon dispersion curves at 25 GPa, and (d) phonon density of states at 25 GPa.

$e_{zz}^{P,T}/e_{xx}^{P,T}$. After that, the HTHP crystal configuration for orthorhombic $MgSiO_3$ pv can be determined from Eq. (16) by using these calculated values of $e_{xx}^{p}(T)$, b, c. It is worth noticing that the error for $MgSiO_3$ pv lattice parameters from this step in our present calculations is on average 0.3%. Such accuracy is sufficient, therefore, no further iterative calculations were carried out in this case.

B. Temperature and pressure dependent elastic constants of orthorhombic $MgSiO_3$ pv

After the optimized lattice parameters have been obtained by using the GOMASC method, the HTHP elastic constants of orthorhombic $MgSiO_3$ pv have been further studied in this work. Since there are 9 independent elastic constants for orthorhombic $MgSiO_3$ pv, 9 independent strain tensors have been applied here. The details on strain tensors for crystal with different symmetry have been listed in Table II.

By using the polynomial fitting technique, second order strain derivatives of the Helmholtz free energy have been obtained, and a series of functional relationships between second order strain derivatives of the Helmholtz free energy and LCIEC have been built. The isothermal elastic constants for orthorhombic $MgSiO_3$ pv have finally been obtained by solving the resulting system of linear equations.

Based on the Eqs. (14) and (15), and the calculated isothermal elastic constants, isentropic elastic constants for orthorhombic $MgSiO_3$ pv have also been calculated.

C. Details of first principles calculations

In this work, first-principles calculations have been carried out by the Vienna *ab initio* simulation package (VASP).[85–87] The $MgSiO_3$ pv conventional cell used in the calculation has 20 atoms; it belongs to the space group *pbmn*. The local density approximation (LDA) has been used for describing the exchange-correction functional.[88,89] Full potential frozen-core projector augmented wave (PAW) describes ion-electron interactions with cutoff energy of 400 eV.[90] The Brillouin zone of the unit cells has been sampled by $3 \times 3 \times 2$ **k**-point mesh. Density of phonon state calculation have been carried out by PHONOPY codes,[91,92] and the supercell approach[93] has been employed, and $1 \times 1 \times 1$ $MgSiO_3$ pv supercells are used in this work. In the phonon frequency calculation, a set of supercells is built with different displacements of the inner atoms. Then, in the supercells, after one atom is displaced, the forces on the atoms are calculated. According to the collected sets of forces, phonon frequencies are obtained. For the elastic constants calculation, 5 strains with maximum strain value of 1.5% is applied for each deformation mode.

D. Results and discussion

Phonon dispersion curve is important for that by calculating phonon dispersion curve, the Helmholtz free energy and other thermodynamic properties can be derived. We calculated the phonon dispersion curve and partial density of

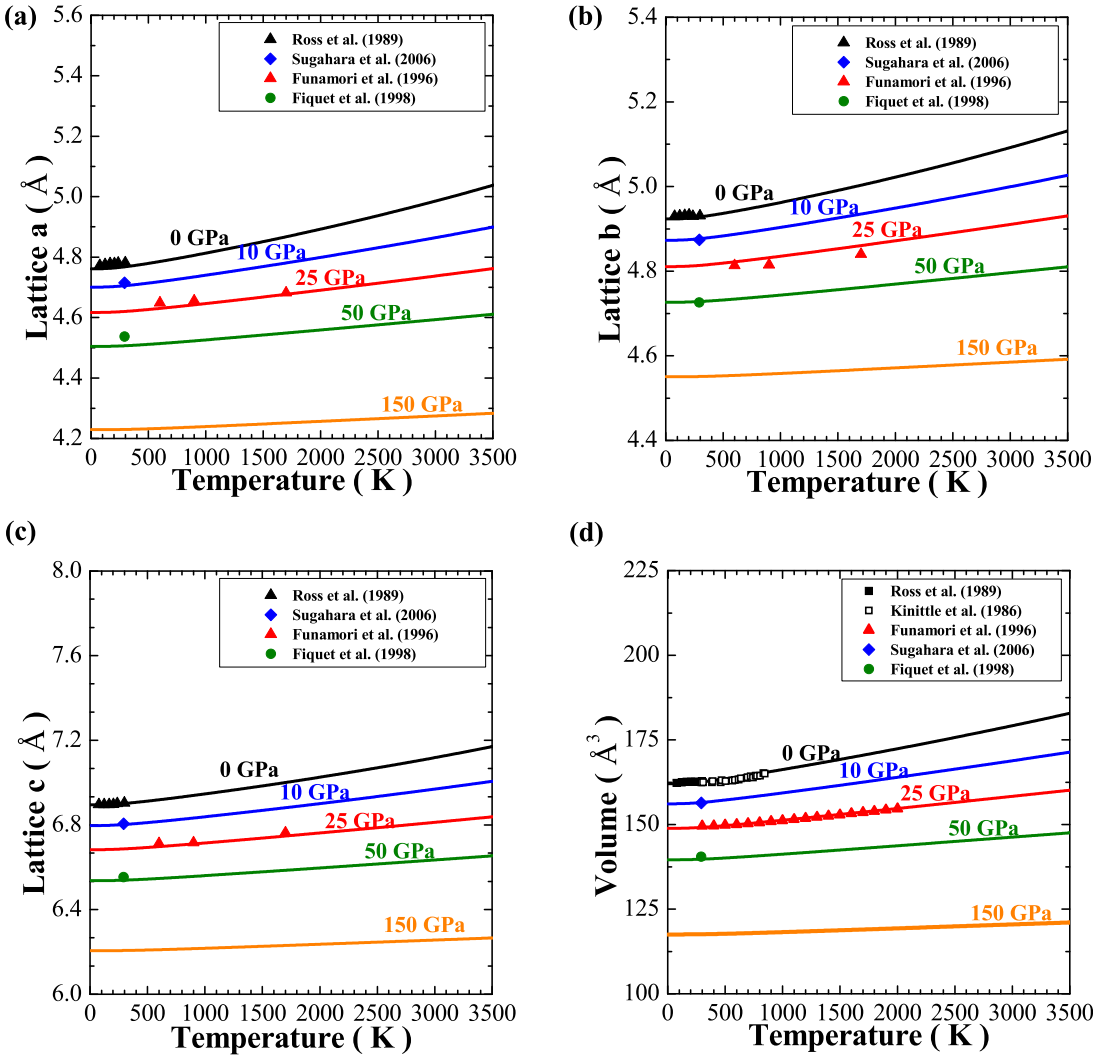

FIG. 2. Comparisons of calculated lattice constant a (a), lattice constant b (b), lattice constant c (c), and cell volume (d) with experimental values.[50–54]

state (PDOS) of $MgSiO_3$ pv at 0 GPa and 25 GPa, respectively. For the $MgSiO_3$ pv unit cell, the 20 atoms in the unit cell corresponding to the 60 vibration modes including 3 acoustic modes and 57 optical modes in the Billouin zone. As shown in Figure 1(a), the phonon band spectra of $MgSiO_3$ pv at 0 GPa accords well with Karki *et al.*[25] and Metsue and Tsuchiya work.[67,68] At 25 GPa, as shown in Figure 1(c), the phonon vibration frequency shift to the higher frequency. At Γ point, the highest optic mode frequency is 1039.88 cm^{-1} for $MgSiO_3$ pv at 0 GPa which agrees with 1032.65 cm^{-1} in Metsue and Tsuchiya work. At 25 GPa, the highest optical mode frequency at Γ point increase up to the 1104.96 cm^{-1}. The pressure has similar effects on phonon dispersion curve compared to Karki *et al.*'s work. In the Figures 1(b) and 1(d), the phonon density of state for $MgSiO_3$ pv at 0 GPa and 25 GPa are shown, respectively. Since the O, Mg, and Si have similar atom weight, due to the highest percent of O atom in the unit cell, the O atom contribute the majority vibration states to the total PDOS at both 0 GPa and 25 GPa.

Based on the obtained phonon dispersion curve, according to Eqs. (9) and (10), the Gibbs function and Helmholtz free energy are obtained. Although LO-TO splitting is ignored by the direct method in our work, the obtained Helmholtz free energy are essentially unaffected by comparing with linear response method,[94,95] therefore the lattice parameter, TEC and elastic constants calculation on the basis of Helmholtz free energy is almost unaffected by neglecting LO-TO splitting in the direct method.

In this work, the lattice parameters of $MgSiO_3$ pv have been calculated by using our newly developed GOMASC method under pressures of 0, 10, 25, 50, 100, and 150 GPa and the temperature range between 0 and 3500 K, and these results have been compared to available experimental values,[50–55] as shown in Figure 2. It can be seen in Figure 2 that the calculated lattice parameters are in a good agreement with the available experimental values, and lattice parameters *a*, *b*, and *c* increase with the increase of temperature but decrease with the increase of pressure. To compare the difference between our present calculated and available experimental values of lattice parameters, we present details on all such values in Table III. As can be seen from Table III, the difference between calculated and experimental values is quite small. By statistical analysis, the average error of our calculated values in comparison with experimental values is about 0.3%, and the maximum error is about 0.6% for the

TABLE III. Comparison of predicted temperature and pressure dependent lattice parameters of $MgSiO_3$ pv with experimental values.

		a (Å)			*b* (Å)			*c* (Å)			*V* (Å^3)			
T (K)	P (GPa)	Calc.[a]	Expt.[b]	Devi.[c]	Calc.[a]	Expt.[b]	Devi.[c]	Calc.[a]	Expt.[b]	Devi.[c]	Calc.[a]	Expt.[b]	Devi.[c]	Refs.
298	0	4.7682	4.782	−0.00289	4.9281	4.931	−0.00059	6.9016	6.904	−0.00035	162.6	162.81	−0.00129	50
238	0	4.7654	4.781	−0.00326	4.9262	4.93	−0.00077	6.8990	6.902	−0.00043	162.38	162.68	−0.00184	50
203	0	4.7641	4.779	−0.00312	4.9252	4.933	−0.00158	6.8978	6.898	−0.00003	162.27	162.63	−0.00221	50
166	0	4.7630	4.779	−0.00335	4.9243	4.932	−0.00156	6.8966	6.897	−0.00006	162.18	162.58	−0.00246	50
123	0	4.7620	4.776	−0.00293	4.9236	4.931	−0.00150	6.8957	6.897	−0.00019	162.14	162.42	−0.00172	50
77	0	4.7615	4.773	−0.00241	4.9232	4.93	−0.00138	6.8951	6.896	−0.00013	162.06	162.26	−0.00123	50
293	10	4.7054	4.7148	−0.00199	4.9023	4.8741	0.00579	6.8020	6.8051	−0.00046	156.9	156.38	0.00333	52
600	25	4.6303	4.6488	−0.00398	4.822	4.8134	0.00179	6.6976	6.7131	−0.00231	149.53	150.22	−0.00460	53
900	25	4.6422	4.6555	−0.00286	4.8318	4.8152	0.00345	6.7104	6.7166	−0.00092	150.52	150.57	−0.00033	53
1700	25	4.6769	4.6823	−0.00115	4.8604	4.8402	0.00417	6.7475	6.7638	−0.00241	153.39	153.29	0.00065	53
293	50	4.5067	4.5368	−0.00663	4.7281	4.726	0.00044	6.5390	6.5532	−0.00217	139.34	140.51	−0.00833	54
Average deviation				0.00314			0.00209			0.00086			0.00254	
Maximum deviation				0.00663			0.00579			0.00241			0.00460	

[a]Calc. is the data from the calculations in the present work.
[b]Expt. is the data from the experimental work, the reference where experimental data is taken from is listed in the right column.
[c]Devi. represents the deviation of the calculated results from the experimental ones, calculated according to the formula $\frac{d_{Calc.}-d_{Expt.}}{d_{Expt.}}$, where $d_{Calc.}$ and $d_{Expt.}$ are the calculated and experimental lattice parameter values, respectively.

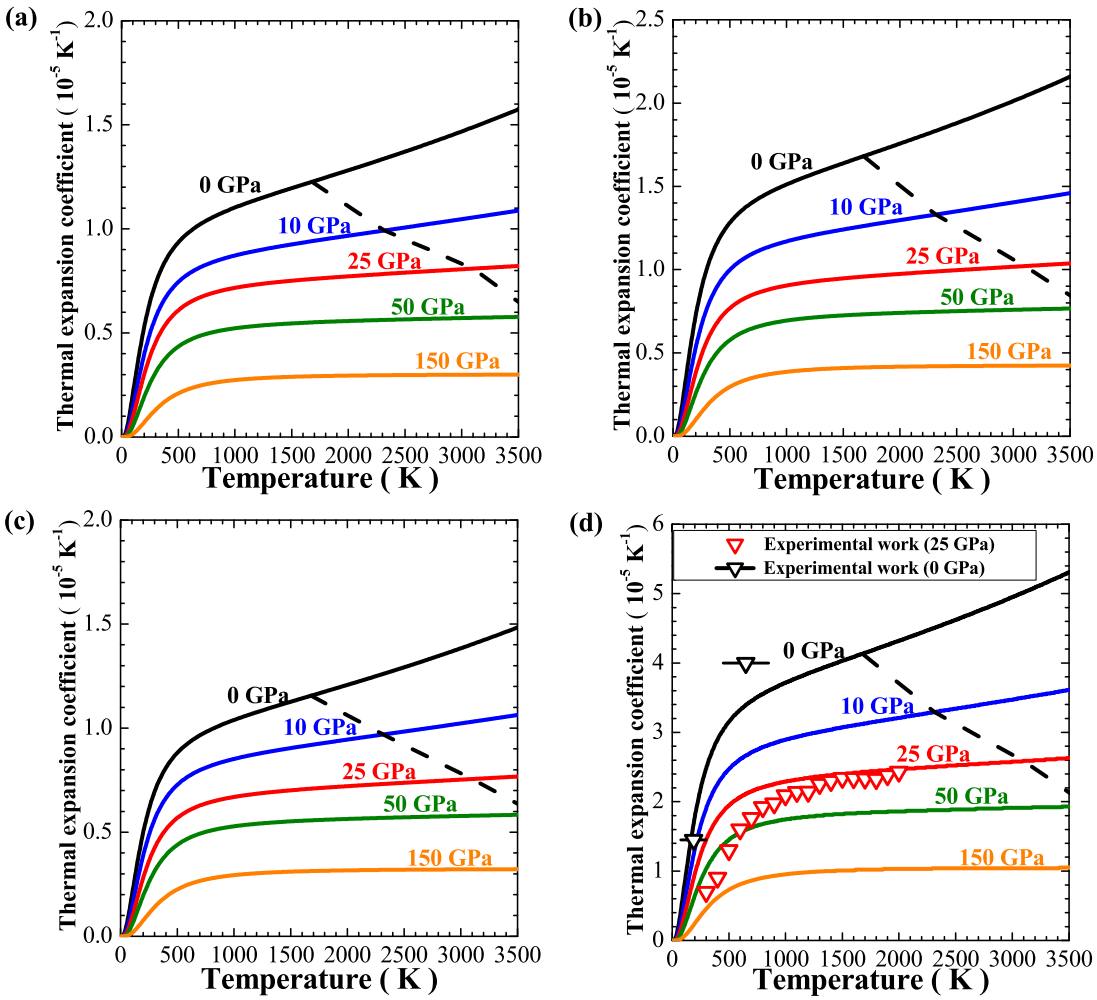

FIG. 3. Comparisons of linear TEC along lattice a direction (a), lattice b direction (b), lattice c direction (c) and volume TEC (d) with experimental values.[50,52,54]

TABLE IV. Calculated linear thermal expansion coefficient of $MgSiO_3$ pv and Beryllium.[a]

Material	T(K)	P(GPa)	α_a 10^{-5} K^{-1}	α_b 10^{-5} K^{-1}	α_c 10^{-5} K^{-1}	Material	T(K) Expt.[75]	α_a 10^{-5} K^{-1}	α_c 10^{-5} K^{-1}	T(K) Calc.[32]	α_a 10^{-5} K^{-1}	α_c 10^{-5} K^{-1}
$MgSiO_3$ pv	1000	0	1.10	1.51	1.04	Beryllium	573	1.57	1.21	200	0.886	0.665
	2000	0	1.28	1.76	1.21		673	1.65	1.28	400	1.77	1.35
	3000	0	1.47	2.01	1.38		773	1.72	1.33	600	2.05	1.62
	1000	25	0.717	0.905	0.669		873	1.78	1.38	800	2.15	1.77
	2000	25	0.772	0.975	0.721		973	1.83	1.43	1000	2.19	1.87
	3000	25	0.806	0.102	0.753		1073	1.87	1.48	1200	2.20	1.95

[a]The calculated data for Beryllium is from the Ref. 32; the experimental data for Beryllium is from the Ref. 96.

given values of lattice *a* and lattice *b*. But for the lattice constant *c*, the average error is about 0.1%, and the maximum error is about 0.3%. For the calculated volume values, the average error is about 0.25%, the maximum error is about 0.5%. These results indicate that our GOMASC method, even without further iterative calculations, provide sufficient accuracy for HTHP crystal geometry optimization. As a result, the computational time is economized to optimize HTHP crystal structures by using our GOMASC method.

In Figure 3, linear TEC for $MgSiO_3$ pv along different lattice directions are displayed and the dotted lines are the inflection points of TEC which represent the boundary for the validity of the QHA model. These calculated results imply that orthorhombic $MgSiO_3$ pv thermal expansion is anisotropic. They also indicate that the temperature domain of validity of QHA widens with the increase in pressure. In our computation, it is found that the ratios of $e^P_{yy}(T)$, $e^P_{zz}(T)$ to $e^P_{xx}(T)$ do not vary significantly over a wide range of

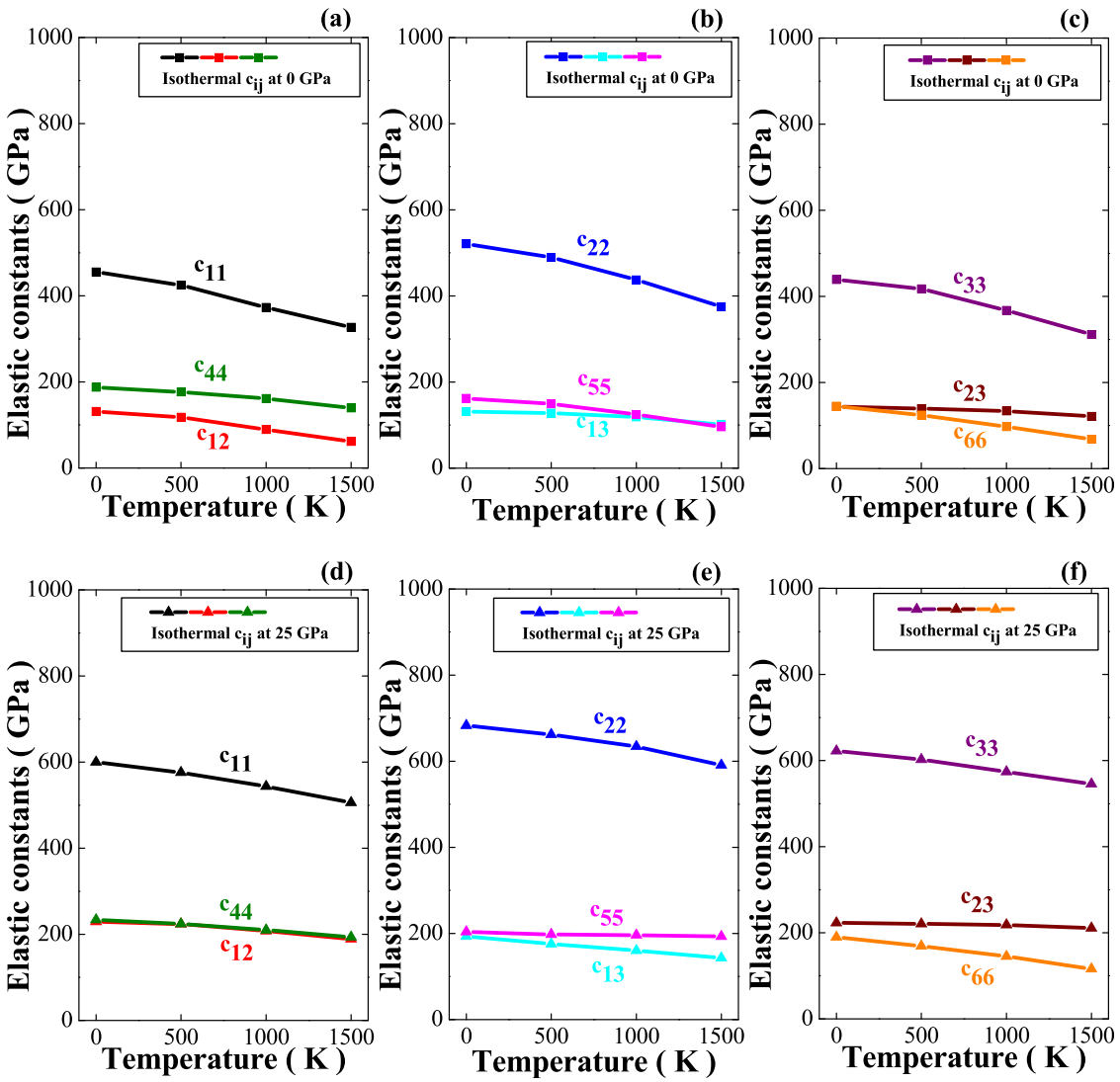

FIG. 4. Isothermal elastic constants of $MgSiO_3$ pv at 0 GPa ((a), (b), (c)) and 25 GPa ((d), (e), (f)).

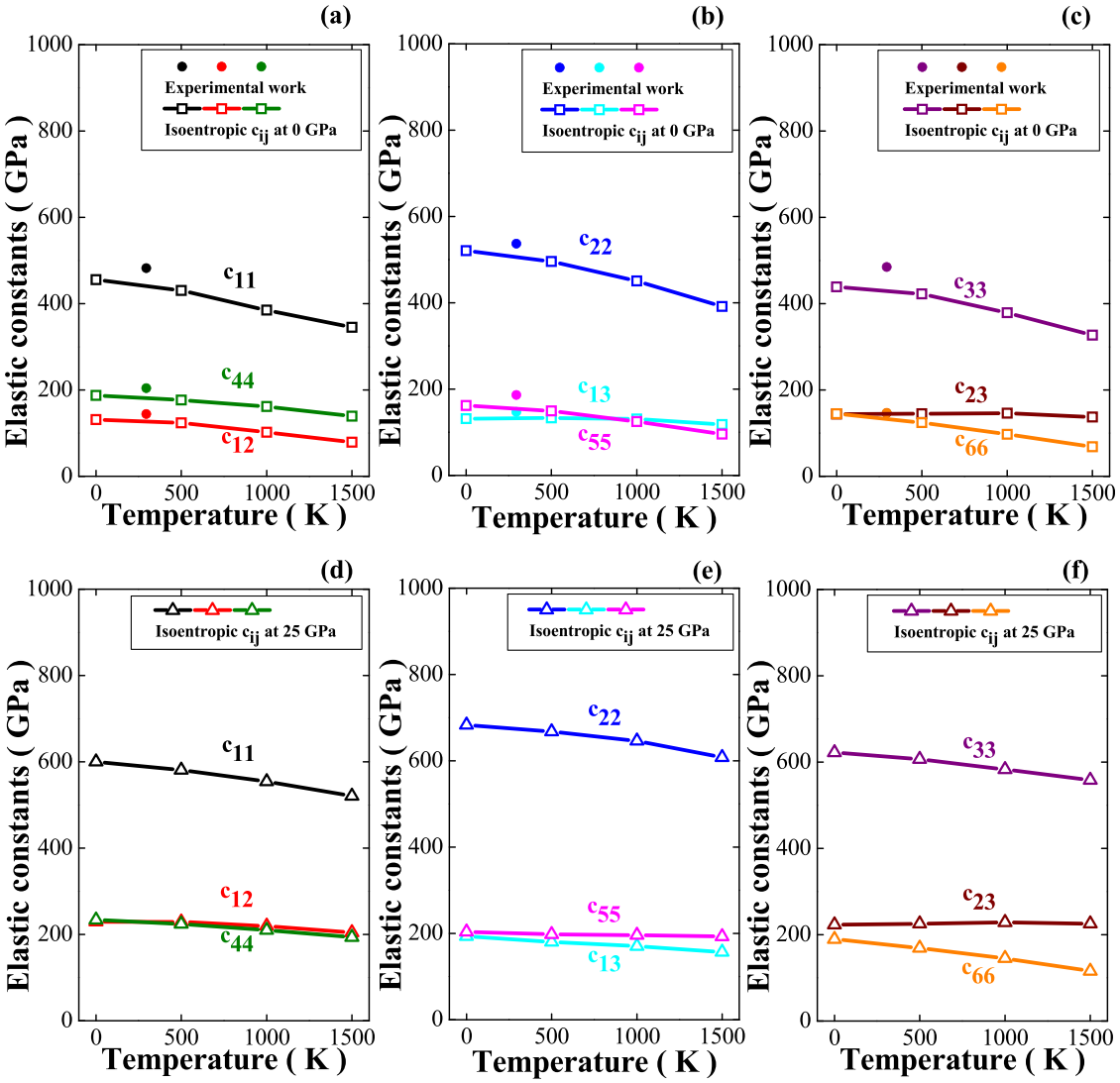

FIG. 5. Comparisons of calculated isentropic elastic constants of $MgSiO_3$ pv at 0 GPa ((a), (b), (c)) and 25 GPa ((d), (e), (f)) with available experimental values (solid circles).[56]

temperatures, indicating that our hypothesis is sound to describe the anisotropic thermal expansion behavior of materials. This can been found in Table IV, with the variation of temperature, the ratio of linear thermal expansion coefficients $\alpha_b^P(T)$ and $\alpha_c^P(T)$ versus $\alpha_a^P(T)$ for orthorhombic lattice $MgSiO_3$ pv and the ratio of $\alpha_c^P(T)$ versus $\alpha_a^P(T)$ for hexagonal lattice Beryllium[32,96] do not change largely with the temperature. Figure 3(d) shows the temperature dependent volume TEC compared with the available experimental TEC values.[50,52,54] It can be seen that the calculated volume TECs agree well with the experimental ones. These results further imply that our calculating method is sound.

In this paper, both isothermal and isentropic elastic constants of orthorhombic $MgSiO_3$ pv have been calculated, as shown in Figures 4 and 5, respectively. Details of comparisons between the calculated, Oganov *et al.*'s *ab initio*

TABLE V. Comparison of calculated isentropic and isothermal elastic constants of $MgSiO_3$ pv with experimental values[56] and *ab initio* calculated values.[60]

T(K)	P(GPa)	Method	c_{11}	C_{12}	c_{13}	c_{22}	c_{23}	c_{33}	c_{44}	c_{55}	c_{66}
298	0	Expt.[56]	482	144	147	537	146	485	204	186	147
0	0	Calc.[60]	492	550	472	142	148	160	213	187	154
0	0	c_{ij}^S/c_{ij}^T	455.6	131.5	131.4	520.5	144.8	438.9	187.4	162.1	144.8
1500	0	c_{ij}^T	326.9	61.5	101.1	374.8	121.3	311.6	139.3	95.5	88.0
1500	0	c_{ij}^S	345.4	79.0	118.0	391.4	137.3	327.1	139.3	95.5	88.0
0	25	c_{ij}^S/c_{ij}^T	600.0	229.2	193.1	591.0	210.7	622.1	233.8	193.1	189.5
1500	25	c_{ij}^T	505.8	188.7	142.9	591.0	210.7	545.4	193.6	142.9	116.0
1500	25	c_{ij}^S	520.5	204.4	156.7	607.8	225.4	558.4	193.6	142.9	116.0

calculation work[60] and experimental elastic constants are listed in Table V.[56] As shown in Figures 4, all isothermal elastic constants decrease with the increase in temperature at both pressures, 0 and 25 GPa. But for isentropic elastic constants, as shown in Figure 5, at pressure 0 GPa, with the increase in temperature from 0 K to 1500 K, the isentropic elastic constants c_{11}, c_{12}, c_{44}, c_{22}, c_{13}, c_{55}, c_{33}, c_{23}, c_{66} soften by 24.2%, 39.9%, 25.7%, 24.8%, 10.2%, 41.1%, 25.5%, 5.2%, and 39.2%, respectively. At pressure of 25 GPa, with the increase in temperature from 0 K to 1500 K, the decreasing magnitude for isentropic elastic constants c_{11}, c_{12}, c_{44}, c_{22}, c_{13}, c_{55}, c_{33}, c_{66}, c_{23} are 13.2%, 10.8% and 17.2% 11.0%, 18.9%, 26.0%, 10.2%, 38.8%, and −1.1% respectively. These results indicate that with the increase of pressure, the isentropic elastic constants resistance toward the increase in temperature is increasing. In Figure 5, the comparisons between the calculated and experimental elastic constants indicate that our calculated isentropic elastic constants are in a good agreement with the experimental ones. These results further confirm that our GOMASC method is effective and sound.

In addition, the c_{23} was observed to be abnormally strengthened by 1.1% with the increase of the temperature from 0 K to 1500 K. The c_{23} in this work describe the resistance of the unit cell against the deformation which rotates around the z axis. With the increase of temperature, due to the change of the c/a or c/b in $MgSiO_3$ pv structure, c_{23} might increase with the temperature. The c_{23}'s abnormal increase behavior with the increase of temperature was also found in other works.[30,57] Also, it was predicted that the elastic constant c_{11} and c_{12} of hcp iron of the Earth's inner core also increased with the increase of temperature.[97]

IV. CONCLUSIONS

In conclusion, we have proposed a methodology called the "geometry optimization method for arbitrary symmetry crystals" to perform HTHP lattice parameters optimization for crystals of arbitrary symmetry. In this method, a series of deformation tensors have been applied, and the corresponding non-equilibrium Gibbs energy functions have been constructed. By minimizing non-equilibrium Gibbs energy functions, the components of deformation tensors, describing deformation, can be determined, and the high temperature and high pressure crystal lattice parameters can be obtained. On the basis of our optimized crystal lattice parameters at high temperature and high pressure conditions, the new computational method for determining the HTHP elastic constants for arbitrary symmetry crystals has been deduced by using Zhao's method. To verify the effectiveness of the developed "geometry optimization method for arbitrary symmetry crystals," we have applied our method to orthorhombic symmetry $MgSiO_3$ pv, and a good agreement between calculated and experimental results has been obtained.

ACKNOWLEDGMENTS

This work was supported by the National Natural Science Foundation of China (Grant No.'s 51121061 and 51131002) and the Key Basic Research Program of Hebei Province of China (No. 12965135D). R.M. acknowledges the support from the NSERC and CRC programs, Canada. The authors also acknowledge the staff of the Center for Computational Materials Science, Institute for Materials Research, Tohoku University, for computer use.

[1]D. Bashford, Acta Astronaut. **22**, 137 (1990).
[2]F. D. Stacey and P. M. Davis, *Physics of the Earth*, 4th ed. (Cambridge University Press, Cambridge, 2008).
[3]W. A. Bassett, T. Takahashi, and P. W. Stook, Review of Scientific Instruments **38**, 37 (1967).
[4]W. A. Bassett, T. Takahashi, H. K. Mao, and J. S. Weaver, J. Appl. Phys. **39**, 319 (1968).
[5]H. K. Mao, W. A. Bassett, and T. Takahashi, J. Appl. Phys. **38**, 272 (1967).
[6]B. E. Brown, Acta Crystal **20**, 268 (1966).
[7]D. Bancroft, E. L. Peterson, and S. Minshall, J. Appl. Phys. **27**, 291 (1956).
[8]R. Kaber, L. Nilsson, N. H. Andersen, A. Lunden, and J. O. Thomas, J. Phys. Condens. Matter **4**, 1925 (1992).
[9]G. Y. Shen, H. K. Mao, R. J. Hemley, T. S. Duffy, and M. L. Rivers, Geophys. Res. Lett. **25**, 373, doi:10.1029/97GL03776 (1998).
[10]C. S. Yoo, H. Kohlmann, H. Cynn, M. F. Nicol, V. Iota, and T. LeBihan, Phys. Rev. B **65**, 104103 (2002).
[11]J. F. Lin, O. Degtyareva, C. T. Prewitt, P. Dera, N. Sata, E. Gregoryanz, H. K. Mao, and R. J. Hemley, Nature **3**, 389 (2004).
[12]A. Dewaele, F. Datchi, P. Loubeyre, and M. Mezouar, Phys. Rev. B **77**, 094106 (2008).
[13]R. A. Felice, J. Trivisonno, and D. E. Schuele, Phys. Rev. B **16**, 5173 (1977).
[14]G. Li and J. R. Gladden, Int. J. Spectrosc. **2010**, 206362 (2010).
[15]R. M. Wentzcovitch, Y. Yu, and Z. Wu, Rev. Mineral. Geochem. **71**, 59 (2010).
[16]R. M. Wentzcovitch, Z. Wu, and P. Carrier, Rev. Mineral. Geochem. **71**, 99 (2010).
[17]A. Debernardi, M. Alouani, and H. Dreyssé, Phys. Rev. B **63**, 064305 (2001).
[18]P. Pavone, K. Karch, O. Schiitt, W. Windl, D. Strauch, P. Giannozzi, and S. Baroni, Phys. Rev. B **48**, 3156 (1993).
[19]B. B. Karki, R. M. Wentzcovitch. S. de Gironcoli, and S. Baroni, Science **286**, 1705 (1999).
[20]B. B. Karki, R. M. Wentzcovitch, S. de Gironcoli, and S. Baroni, Phys. Rev. B **61**, 8793 (2000).
[21]Y. Wang, Z. K. Liu, and L. Q. Chen, Acta Mater. **52**, 2665 (2004).
[22]A. Togo, L. Chaput, I. Tanaka, and G. Hug, Phys. Rev. B **81**, 174301 (2010).
[23]S. L. Shang, H. Zhang, Y. Wang, and Z. K. Liu, J. Phys.: Condens. Matter **22**, 375403 (2010).
[24]J. Althoff, P. Allen, R. Wentzcovich, and J. A. Moriarty, Phys. Rev. B **48**, 13253 (1993).
[25]B. B. Karki, R. M. Wentzcovitch, S. de Gironcoli, and S. Baroni, Phys. Rev. B **62**, 14750 (2000).
[26]Z. Wu and R. M. Wentzcovitch, Phys. Rev. B **79**, 104304 (2009).
[27]Z. Wu and R. M. Wentzcovitch, Phys. Rev. B **83**, 184115 (2011).
[28]P. Carrier, R. M. Wentzcovitch, and J. Tsuchiya, Phys. Rev. B **76**, 064116 (2007).
[29]P. Carrier, J. F. Justo, and R. M. Wentzcovitch, Phys. Rev. B **78**, 144302 (2008).
[30]R. M. Wentzcovitch, B. B. Karki, M. Cococcioni, and S. de Gironcoli, Phys. Rev. Lett. **92**, 018501 (2004).
[31]R. M. Wentzcovitch, T. Tsuchiya, and J. Tsuchiya, Proc. Natl. Acad. Sci. U.S.A. **103**, 543 (2006).
[32]T. Shao, B. Wen, R. Melnik, S. Yao, Y. Kawazoe, and Y. Tian, J. Appl. Phys. **111**, 083525 (2012).
[33]T. H. Jordan, Proc. Natl. Acad. Sci. U.S.A. **76**, 4192 (1979).
[34]*Earth's Deep Interior: Mineral Physics and Tomography From the Atomic to the Global Scale*, edited by S. Karato, A. Forte, R. Liebermann, G. Masters, and L. Stixrude, Geophysics Monograph Series, (AGU, Washington, D. C., 2000), Vol. 117, p. 289.
[35]N. Kawai, M. Tachimori, and E. Ito, Proc. Jpn. Acad. **50**, 378 (1974).
[36]E. Ito and Y. Matsui, Phys. Earth Planet. Interior **9**, 344 (1974).
[37]E. Ito and H. Yamada, in *High-Pressure Research in Geophysics*, edited by S. Akimoto and M. H. Manghnani (D. Reidel, Norwell, Mass, 1982), pp. 405–419.

[38]H. Horiuchi, M. Hirano, E. Ito, and Y. Matsui, Am. Mineral. **67**, 788 (1982).
[39]T. Gasparik, J. Geophys. Res. **95**, 15751 (1990).
[40]B. B. Karki and R. M. Wentzcovitch, J. Geophys. Res. **107**, 2267, doi: 10.1029/2001JB000702 (2002).
[41]L. G. Liu, Geophys. Res. Lett. **1**, 277, doi:10.1029/GL001i006p00277 (1974).
[42]L. G. Liu, Nature **258**, 510 (1975).
[43]E. Knittle and R. Jeanloz, Science **235**, 668 (1987).
[44]L. Stixrude and R. E. Cohen, Nature **364**, 613 (1993).
[45]Ph. D'Arco, G. Sandrone, R. Dovesi, E. April, and V. R. Saunders, Phys. Chem. Miner. **21**, 285 (1994).
[46]B. B. Karki, W. Duan, C. R. S. da Silva, and R. M. Wentzcovitch, Am. Mineral. **85**, 317 (2000).
[47]A. R. Oganov and S. Ono, Nature **430**, 445 (2004).
[48]M. Murakami, K. Hirose, K. Kawamura, N. Sata, and Y. Ohishi, Science **304**, 855 (2004).
[49]T. Tsuchiya, J. Tsuchiya, S. Umemoto, and R. M. Wentzcovitch, Earth Planet. Sci. Lett. **224**, 241 (2004).
[50]N. Ross and R. Hazen, Phys. Chem. Miner. **16**, 415 (1989).
[51]E. Knittle, R. Jeanloz, and G. L. Smith, Nature **319**, 214 (1986).
[52]M. Sugahara, A. Yoshiasa, Y. Komatsu, T. Yamanaka, N. Bolfan-Casanova, A. Nakatsuka, S. Sasaki, and M. Tanaka, Am. Mineral. **91**, 533 (2006).
[53]N. Funamori, T. Yagi, W. Utsumi, T. Kondo, T. Ushida, and M. Funamori, J. Geophys. Res. **101**, 8257, doi:10.1029/95JB03732 (1996).
[54]G. Fiquet, D. Andrault, A. Dewaele, T. Charpin, M. Kunz, and D. Hausermann, Phys. Earth Planet. Interior **105**, 21 (1998).
[55]H. Horiuchi, E. Ito, and D. J. Weidner, Am. Mineral. **72**, 357 (1987).
[56]A. Yeganeh-Haeri, Phys. Earth Planet. Interior **87**, 111 (1994).
[57]T. Yamanaka, Y. Komatsu, M. Sugahara, and T. Nagai, Am. Mineral. **90**, 1301 (2005).
[58]S. Ono, T. Kikegawa, and Y. Ohishi, Am. Mineral. **91**, 475 (2006).
[59]A. R. Oganov, J. P. Brodholt, and G. D. Price, Nature **411**, 934 (2001).
[60]A. R. Oganov, J. P. Brodholt, and G. D. Price, Earth Planet. Sci. Lett. **184**, 555 (2001).
[61]N. Shimobayashi, A. Miyake, M. Kitamura, and E. Miura, Phys. Chem. Miner. **28**, 591 (2001).
[62]X. Gonzea, J. M. Beukena, R. Caracasa, F. Detrauxa, M. Fuchsa, G. M. Rignanesea, L. Sindica, M. Verstraetea, G. Zerahb, F. Jolletb, M. Torrentb, A. Royb, M. Mikamic, Ph. Ghosezd, J. Y. Ratyd, and D. C. Allane, Comput. Mater. Sci. **25**, 478 (2002).
[63]S. Qin and R. C. Wang, Acta Geol. Sin. **78**, 345 (2004).
[64]R. M. Thompson and R. T. Downs, Am. Mineral. **89**, 614 (2004).
[65]S. Jahn and R. Martonak, Am. Mineral. **94**, 950 (2009).
[66]J. Tsuchiya, T. Tsuchiya, and R. M. Wentzcovitch, J. Geophys. Res. **110**, B02204, doi:10.1029/2004JB003409 (2005).
[67]A. Metsue and T. Tsuchiya, J. Geophys. Res. **116**, B08207, doi:10.1029/2010JB008018 (2011).
[68]A. Metsue and T. Tsuchiya, Geophys. J. Int. **190**, 310 (2012).
[69]J. F. Nye, *Physical Properties of Crystals: Their Representation by Tensors and Matrices* (Oxford University Press, Oxford, 1967).
[70]J. F. Smith, J. Phase Equilib. Diffus. **25**, 405 (2004).
[71]O. L. Anderson, *Equations of State of Solids for Geophysics and Ceramic Science* (Oxford University Press, New York, 1995).
[72]A. A. Maradudin, E. W. Montroll, G. H. Weiss, and I. P. Ipatova, *Theory of Lattice Dynamics in the Harmonic Approximation* (Academic, New York, 1971).
[73]K. Parlinski, J. Phys.: Conf. Ser. **92**, 012009 (2007).
[74]A. B. Belonoshko, S. Arapan, and A. Rosengren, J. Phys.: Condens. Matter **23**, 485402 (2011).
[75]J. M. Dickey and A. Paskin, Phys. Rev. **188**, 1407 (1969).
[76]J. Wang, J. Li, S. Yip, S. Phillpot, and D. Wolf, Phys. Rev. B **52**, 12627 (1995).
[77]J. J. Zhao, J. M. Winey, and Y. M. Gupta, Phys. Rev. B **75**, 094105 (2007).
[78]R. N. Thurston, *in Physical Acoustics Principles and Methods*, edited by W. P. Mason and R. N. Thurston (Academic, New York, 1964), Vol. 1A, p. 1.
[79]D. C. Wallace, in *Solid State Physics*, edited by F. Seitz and D. Turnbull (Academic, New York, 1970), Vol. 25, p. 301.
[80]M. Catti, Acta Crystallogr. **41**, 494 (1985).
[81]T. C. T. Ting, *Anisotropic Elasticity—Theory and Applications* (Oxford University Press, Oxford, 1996).
[82]G. Steinle-Neumann, L. Stixrude, and R. E. Cohen, Phys. Rev. B **60**, 791 (1999).
[83]C. Asker, L. Vitos, and I. A. Abrikosov, Phys. Rev. B **79**, 214112 (2009).
[84]G. F. Davies, J. Phys. Chem. Solids **35**, 1513 (1974).
[85]G. Kresse, M. Marsman, and J. Furthmüller, *VASP the Guide* (Computational Physics, Faculty of Physics, Universität Wien, Wien, 2011).
[86]G. Kresse and J. Hafner, Phys. Rev. B **47**, 558 (1993).
[87]G. Kresse and J. Furthmuller, Phys. Rev. B **54**, 11169 (1996).
[88]D. M. Ceperley and B. J. Alder, Phys. Rev. Lett. **45**, 566 (1980).
[89]J. P. Perdew and A. Zunger, Phys. Rev. B **23**, 5048 (1981).
[90]P. E. Blöchl, Phys. Rev. B **50**, 17953 (1994).
[91]A. Togo, F. Oba, and I. Tanaka, Phys. Rev. B **78**, 134106 (2008).
[92]A. Togo, Phonopy.
[93]K. Parlinski, Z. Q. Li, and Y. Kawazoe, Phys. Rev. Lett. **78**, 4063 (1997).
[94]D. Alfè, Comput. Phys. Commun. **180**, 2622 (2009).
[95]A. B. Belonoshko, S. Arapan, R. Martonak, and A. Rosengren, Phys. Rev. B **81**, 054110 (2010).
[96]P. Gordon, J. Appl. Phys. **20**, 908 (1949).
[97]G. Steinle-Neumann, L. Stixrude, R. E. Cohen, and O. G. lseren, Nature **413**, 57 (2001).